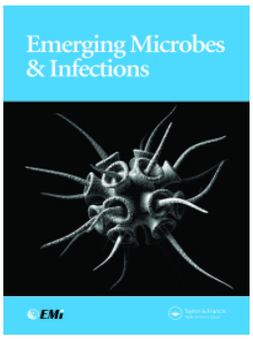

Emerging Microbes & Infections

ISSN: 2222-1751 (Online) Journal homepage: www.tandfonline.com/journals/temi20

Differential innate immune activation by wild-type and NSs-deficient RVFV strains in human blood monocytes

Niranjana Nair, Julia Friese, Paul J. Wichgers Schreur, Albert D. M. E. Osterhaus, Guus F. Rimmelzwaan & Chittappen Kandiyil Prajeeth

To cite this article: Niranjana Nair, Julia Friese, Paul J. Wichgers Schreur, Albert D. M. E. Osterhaus, Guus F. Rimmelzwaan & Chittappen Kandiyil Prajeeth (2026) Differential innate immune activation by wild-type and NSs-deficient RVFV strains in human blood monocytes, Emerging Microbes & Infections, 15:1, 2610855, DOI: 10.1080/22221751.2025.2610855

To link to this article: https://doi.org/10.1080/22221751.2025.2610855

Emerging Microbes & Infections
2026, VOL. 15, 2610855 (15 pages)
https://doi.org/10.1080/22221751.2025.2610855

Differential innate immune activation by wild-type and NSs-deficient RVFV strains in human blood monocytes

Niranjana Nair[a], Julia Friese[a], Paul J. Wichgers Schreur[b], Albert D. M. E. Osterhaus[a], Guus F. Rimmelzwaan[a]* and Chittappen Kandiyil Prajeeth[a]*

[a]Research Center for Emerging Infections and Zoonoses, University of Veterinary Medicine, Hannover, Germany; [b]Wageningen Bioveterinary Research, Lelystad, Netherlands

ABSTRACT

Rift Valley fever virus (RVFV) is a *Phlebovirus* causing febrile and haemorrhagic illness in ruminants and humans. The viral protein NSs is a major virulence factor that suppresses the IFN-β response in various hosts. Hence, RVFV variants lacking functional NSs, such as Clone 13, are highly attenuated. It is speculated that from the sites of infection, the virus disseminates to the target organs via the bloodstream. We hypothesized that primary infection of circulating immune cells and their response to infection are critical factors determining systemic RVFV spread and pathogenesis. Human PBMC from healthy blood donors were exposed to both wild-type (WT) RVFV and Clone 13 strains. Flow cytometric analysis revealed that monocytes expressing LRP1, a known RVFV receptor, are target cells for RVFV. RNA-seq analysis of monocytes exposed to WT and Clone 13 strains showed a large number of differentially expressed genes compared to mock-exposed cells. Various genes involved in antiviral immune mechanisms were specifically modulated in monocytes either in response to WT or Clone 13 infection. Expression of genes encoding key inflammatory mediators, such as *CCL2*, *CD40*, and *CD83,* was only upregulated in Clone 13-infected monocytes, whereas *IFNB1* and *NFKB1* were downregulated specifically in WT-infected monocytes. Taken together, our findings suggest that RVFV NSs dampen the innate immune responses in monocytes which may be critical not only in RVFV pathogenesis but also in the induction of virus-specific immune response.

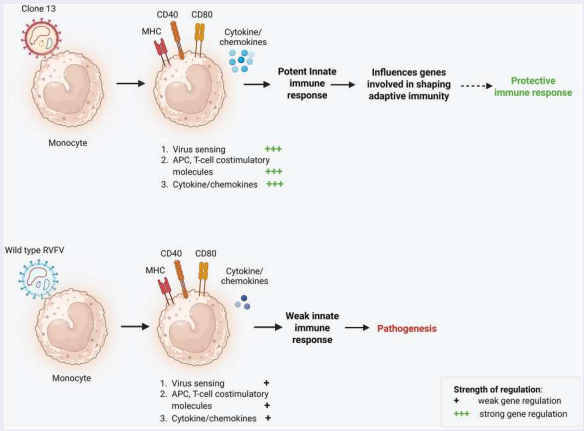

ARTICLE HISTORY Received 26 August 2025; Revised 28 November 2025; Accepted 25 December 2025

KEYWORDS RVFV; NSs; monocyte; immune activation; pathogenesis; cytokine; chemokine

Introduction

Rift Valley fever virus (RVFV), a *Phenuiviridae* family member, was initially identified as a source of abortion storms in sheep in the Rift Valley region of Kenya. Later, the disease was also reported in humans in close contact with diseased livestock [1,2]. It is horizontally transmitted by *Aedes* and *Culex* mosquitoes among livestock, whereas humans are mainly infected by contact with contaminated blood, carcasses or by consumption of unpasteurized milk from infected ruminants. A key characteristic of the disease is abortion storms in ruminants, predominantly in sheep and goats, as well as high mortality in newborn and young animals [3]. Infection outcomes in adult ruminants largely vary from asymptomatic, subclinical infection to severe febrile illness, hepatic disease accompanied

CONTACT Chittappen Kandiyil Prajeeth prajeeth.chittappen.kandiyil@tiho-hannover.de
*Shared senior authors.

Supplemental data for this article can be accessed online at https://doi.org/10.1080/22221751.2025.2610855.

by haemorrhage, multifocal necrosis, and mild splenomegaly [4,5]. Human infections are mostly asymptomatic or manifest as self-limiting febrile illness; 8–10% of symptomatic individuals develop severe disease with hepatic lesions, haemorrhage, encephalitis or ocular disease [5].

The virus genome is a three-segmented negative-sense RNA consisting of the S, M and L segments, which encode several structural and non-structural proteins [6,7]. Non-structural protein NSs encoded by the S segment acts as the major virulence factor of the virus by suppressing host transcription, abrogating type-I interferon response and enabling virus replication [3]. Moreover, NSs form nuclear filaments assembling into amyloid fibrils and contributing to the virulence *in vivo* [8,9]. Mutations in NSs are linked to reduced virulence as observed in natural isolates such as Clone 13 [10–12].

Although various functions of NSs have been identified previously, their contribution to dissemination and pathogenesis, especially in humans, is poorly understood. Moreover, early events leading to virus dissemination from the entry sites to the target organs, such as the liver in humans, remain unclear. It has been shown that macrophages, dendritic cells and granulocytes were infected by Clone 13 in *Ifnar1*-deficient mice, after inoculation by the intraperitoneal route [13]. Human monocyte-derived macrophages were also shown to be susceptible to infection with RVFV *in vitro* [14]. Here, we report that monocytes among peripheral blood mononuclear cells (PBMC) can be infected with RVFV. We further compared the monocyte response to infection with WT and NSs-deficient RVFV strains using a transcriptomics approach and observed major differences that could be critical for viral pathogenesis and host immunity to infection.

Materials and methods

Ethics statement

Buffy coats from healthy blood donors appearing for voluntary blood donation were obtained from Deutsches Rotes Kreuz, Springe, Germany. Written informed consent was obtained from all donors, and the procedure was approved by the Hannover Medical School Ethics Committee (No. 3393-2016).

Methods

Methods are described in detail in the supplementary material and methods (SMM). A brief description of the methods is presented here. Wild-type RVFV strain 35/74 and Clone 13 stocks were generated as described in the SMM. PBMC were isolated by overlaying buffy coats pre-diluted with phosphate-buffered saline (PBS) + 2% FBS solution onto Lymphoprep density gradient medium (18061, StemCell Technologies) in SepMate-50 (IVD) tubes (85450, StemCell Technologies) and centrifuging at 1200 g. PBMC obtained from this procedure were frozen in aliquots and stored at −150°C until further use. PBMC were thawed and resuspended in warm R10F medium. Monocytes were isolated using the classical human monocyte isolation Kit (130-117-337, Miltenyi Biotec) and autoMACS Pro Separator (130-092-545, Miltenyi Biotec) as per manufacturer instructions. The monocytes obtained from this procedure had high purity (>95%) and good viability (Supplementary figure S1a). PBMC and monocytes (1×10^6 and 2×10^6 cells, respectively) were inoculated with RVFV 35/74 and Clone 13 at a multiplicity of infection (MOI) of 1 in infection medium (CIM++ medium) for one hour, following which the initial inoculum was thoroughly washed, and the cells were maintained in culture medium for the specified time. The infectivity was assessed by intracellular staining of PBMC and monocytes for RVFV Nucleoprotein (N) using rabbit-polyclonal anti-N antibody (Genscript) followed by a secondary Donkey anti-Rabbit IgG Alexa Fluor 647 antibody [15]. Flow cytometric characterization of infection among PBMC subpopulations was done using antibodies against cell-specific markers as specified in SMM. RNA was extracted from the infected cells using Qiagen RNeasy mini kit (74104, Qiagen) following the manufacturer's protocol. Copies of RVFV-M gene fragment in the infected monocytes were quantified by RT-qPCR assay using Luna Universal One-Step RT-qPCR Kit (E3005X, New England Biolabs) and forward primer 5'-AAAGGAACAATGGACTCTGGTCA-3' and reverse primer 5'-CACTTCTTACTACCATGTCCTCCAAT-3' as described by Drosten et al. [16]. RNA-seq analysis was performed on total RNA isolated from mock and infected monocytes using Illumina sequencing. Library preparation, bioinformatics pipeline and quantification of gene expression levels are described in detail in SMM. Infectious virus titres in culture supernatants of Clone 13, RVFV 35/74 or mock-infected monocytes collected at 24 hpi were determined in BHK-21 cells and expressed as $TCID_{50}$ per mL. $TCID_{50}$ values were calculated using Reed and Muench method. Concentration of CCL2 and CXCL9 in the culture supernatants was quantified using commercially available ELISA kits (Invitrogen) according to the manufacturer's instructions.

Statistical analysis and RNA-Seq data analysis

Data was analysed using GraphPad Prism version 10.4.1. Statistics for FACS analysis were performed using Two-way ANOVA with Tukey's multiple comparisons test. One-way ANOVA with Kruskal–Wallis test was used for RT-qPCR. p-value <0.05 is

considered as statistically significant. RNA-seq data were analysed using the Novomagic platform of Novogene. DEGs with |Log2 fold change| ≥ 1 and $p < 0.05$ were considered for Gene Ontology (GO), KEGG and Reactome analysis using Novomagic. SRPlot online platform was used for generating dumbbell plots for commonly regulated genes [17]. RaNA-seq was used for interaction network analysis of the top 10 differentially regulated pathways during infection [18].

Results

Human PBMC are susceptible to infection with RVFV

To investigate cell tropism, PBMC isolated from healthy human blood donors were exposed to RVFV strain 35/74 (WT) or to the NSs-deficient RVFV (Clone 13) at an MOI of 1. Comparison of nucleotide and amino acid sequences of Clone 13 and RVFV 35/74 revealed striking homology except for a 69% in-frame deletion in the NSs gene in Clone 13, making it non-functional (Supplementary figure S2). Following culture, the cell viability was slightly reduced in both mock-treated and virus-inoculated PBMC (Figure 1(a)). At 24 h post inoculation (hpi), approximately 8% of PBMC stained positive for RVFV nucleoprotein (N) antigen, hence reflecting similar infectivity of both WT and Clone 13 (Figure 1(b)).

Further flow cytometric characterization of infected PBMC using cell-specific markers identified monocytes as a major cellular target of RVFV (Figure 1(c) & Supplementary figure S3). Among all infected cells at 24 hpi, 42% were $CD14^+$ monocytes, 9% were T cells, whereas B cells and NK cells constituted minor targets for RVFV infection. Thus, among PBMC, monocytes were the primary targets for RVFV infection.

Human monocytes express RVFV receptor LRP1

DC-SIGN, a C-type lectin and low-density lipoprotein receptor-related protein (LRP1) are known entry receptors for RVFV. To investigate whether the preferred cellular tropism of RVFV correlated with the expression of these entry factors, flow cytometry was performed on PBMC. Only a minor population of monocytes ($CD11b^+$ $CD14^+$), B cells ($CD19^+$) and T cells ($CD3^+$) expressed DC-SIGN. Interestingly, LRP1 was highly expressed on monocytes with >88% $CD11b^+$ $CD14^+$ cells staining positive for LRP1. In contrast, LRP1 expression was relatively low on T cells and not expressed on B cells (Figure 2). Taken together, this suggests that RVFV may enter human monocytes by virtue of their LRP1 expression.

RVFV infection of purified human monocytes

To confirm infection of monocytes, MACS-sorted cells were inoculated with WT and Clone 13 at an MOI of 1. Virus-inoculated monocytes showed reduced cell viability at 24 hpi, with viabilities of 67% for WT and 71% for Clone 13 strains. Mock-infected cells maintained a cell viability of >85%, indicating that RVFV infection exerts cytopathic effects in monocytes (Figure 3). Infectivity was assessed at 1 and 24 hpi by flow cytometry using staining to detect intracellular viral N protein. Minor background staining of <0.8% was detected at 1 hpi. The proportion of N^+ monocytes among WT and Clone 13-infected monocytes significantly increased at 24hpi with comparable infection rates (~15% and ~14%, respectively) between both strains. Thus, WT and Clone 13 can infect purified human monocytes to a similar extent, leading to modest loss of viability.

WT RVFV and clone 13 induce differential transcription profiles in infected monocytes

Monocyte response to WT and Clone 13 infections was assessed at the transcription level by RNA-seq analysis on total RNA isolated at 24 hpi (Supplementary figure S1b & S1c shows virus copy number and infectious virus titre at 24 hpi, respectively). In comparison to mock-infected monocytes, expression of 3774 and 3916 genes was significantly altered, greater than two-fold (p-value <0.05) in WT- and Clone 13-infected monocytes (Figure 4). Among these, 1661 genes were commonly expressed after infection with either virus. A significant number of differentially expressed genes (DEG), 2113 in WT and 2255 in Clone 13, were unique to each virus infection, indicating strain-specific host responses (Figure 4(d)). Further analysis of WT infection-induced responses revealed that among the DEG, 79% of genes were downregulated and only 21% were upregulated compared to mock-infected monocytes. In contrast, 55% of DEG were downregulated and 45% genes were upregulated in Clone 13-infected monocytes.

Gene ontology (GO) enrichment analysis was performed using total upregulated and downregulated gene sets to identify biological processes affected in monocytes following WT and Clone 13 infection (Figure 5). GO terms enriched using upregulated genes were predominantly associated with antiviral defence mechanisms, including "response to virus" and "defence response to virus", etc., for both Clone 13 and WT virus infections. Nevertheless, the number of genes associated with each GO term was different between the strains (Supplementary table S1). Another prominent GO term enriched with the upregulated gene set was associated with cytokine activity

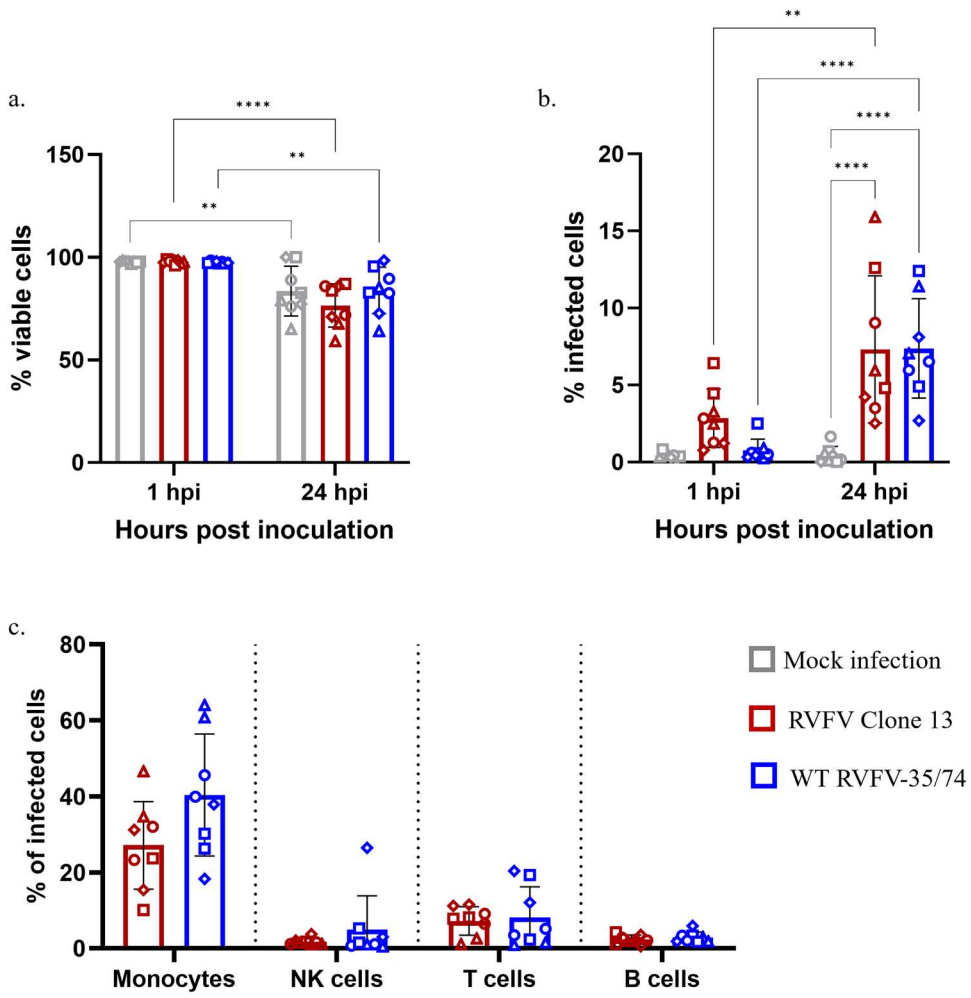

Figure 1. Human PBMC infection with Clone 13 and RVFV 35/74 (WT). a. Cell viability at 1 and 24 hpi expressed as percentage of LIVE/DEAD negative cells. b. Percentage of virus-infected cells in PBMCs as determined by RVFV Nucleoprotein staining at 1 and 24 hpi. c. Subpopulations of infected PBMCs were distinguished based on surface marker expression into monocytes, NK cells, T cells and B cells. The respective treatments are colour coded as indicated (grey, mock-infected; red, Clone 13-infected and blue, WT-infected). Each symbol represents the results obtained with an individual blood donor. Two independent experiments with four donor PBMCs per experiment are shown ($n = 8$). Statistical significance was determined using Two-Way ANOVA with Tukey's multiple comparisons test. $*p < 0.05$; $**p < 0.01$; $***p < 0.001$; $****p < 0.0001$.

and responses to cytokine signalling (Figure 5(a)). For the downregulated gene set, GO-enriched processes were primarily associated with chemotaxis and leukocyte recruitment, suggesting migratory and inflammatory responses are affected following infection with both Clone 13 and WT strains (Figure 5(b)). Network analysis based on the top 10 pathways that demonstrated the highest statistical significance showed a cluster of biologically related processes that were common as well as distinct between infections with either of the viruses. The involvement of "immune pathways" was common in both networks. Notably, Clone 13 infection showed interaction among "innate immune system" and "adaptive immune system", which was absent in WT RVFV-infected monocytes (Figure 5(c,d)). Collectively, the DEG analysis indicates that both viral strains induce an antiviral state in monocytes with Clone 13-infected monocytes showing distinct potential to engage with the adaptive immune system.

Infections with the WT RVFV strain and clone 13 induce different immune activation pathways

To obtain a better understanding of the common pathways, Reactome pathway enrichment analysis was performed on 1661 shared DEG induced by Clone 13 and WT infections (Figure 4(d)). Top pathways selected by high statistical significance were further categorized into groups based on the function possibly affected by these pathways. As demonstrated in Figure 6, the major pathways listed for both strains include the interferon and interleukin signalling pathways along with genes associated with antigen processing and presentation (Figure 6(a,b), Supplementary tables S2 and S3). Using KEGG pathway analysis, gene ratios of the top 16 significant pathways regulating the innate immune responses in monocytes were compared for Clone 13 and WT infection, including those involved in antigen processing and presentation, B-cell and T cell receptor signalling, RIG-I-like

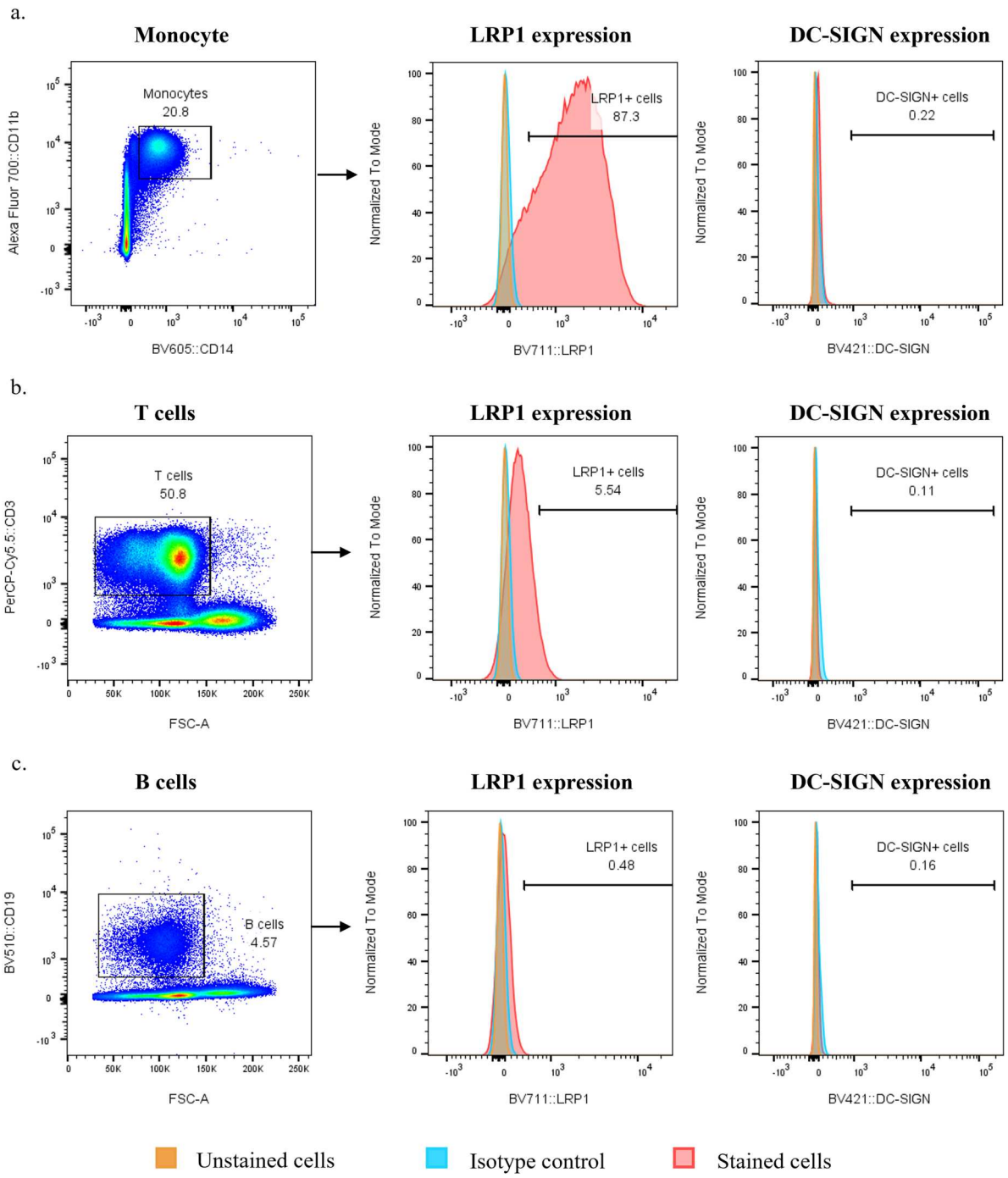

Experiment	Donor No.	Percentage of LRP1+ cells in individual subpopulations		
		Monocytes	B cells	T cells
1	Donor 1	85.50%	4.18%	9.49%
	Donor 2	94.00%	0.68%	6.80%
	Donor 3	97.20%	0.48%	7.67%
	Donor 4	95.70%	0.60%	3.12%
2	Donor 1	75.80%	2.54%	6.01%
	Donor 2	83.50%	1.16%	4.36%
	Donor 3	91.20%	0.57%	3.95%
	Donor 4	84.70%	1.31%	2.52%
	Average	**88.45%**	1.44%	5.49%

Figure 2. Expression of putative RVFV entry receptors on PBMC populations. Representative FACS plots of LRP1 and DC-SIGN expression on a. monocytes, b. T cells and c. B cells. Colours indicate antibody staining of cells (orange, unstained cells; blue, isotype control; red, receptor-specific antibody-stained cells). Two independent experiments with four donor PBMC per experiment are shown ($n = 8$).

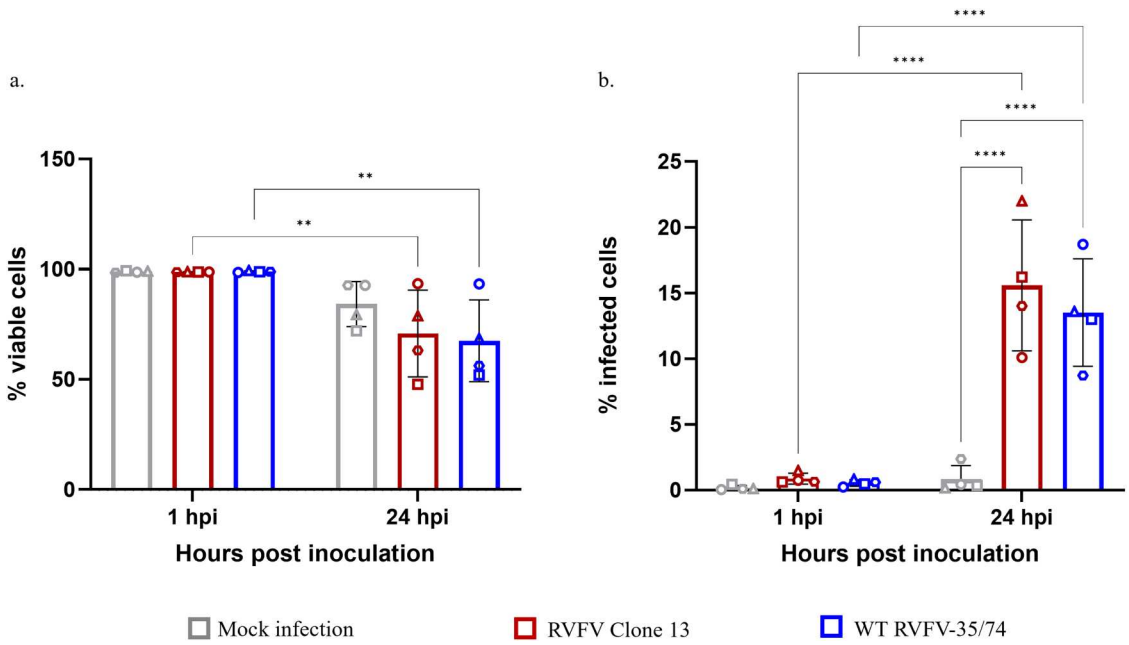

Figure 3. RVFV infection of purified monocytes. a. Percentage of viable cells, b. infected monocytes after 1 and 24 hpi measured by flow cytometry. Each data point represents monocytes from an individual blood donor ($n = 4$) that were mock-infected (grey) or infected with Clone 13 (red) or WT (blue) virus. Statistical significance was determined using two-way ANOVA with Tukey's multiple comparisons test. $*p < 0.05$; $**p < 0.01$; $***p < 0.001$; $****p < 0.0001$.

receptor signalling, NF-κB signalling and MAPK signalling (Figure 6(c), Supplementary table S4). The gene ratios show that Clone 13-infected monocytes had a higher number of genes associated with these pathways, satisfying the selection criteria of >10 genes per pathway with p-value <0.05, compared to monocytes infected with the WT virus. Although the monocyte response to infection with either virus was similar, the degree and nature of gene expression varied.

To compare the magnitude of the response to Clone 13 and WT infections, we assessed the fold changes, relative to mock controls, in selected genes involved in innate immunity and in shaping adaptive immune response, including several chemokines and cytokines, costimulatory molecules and transcription factors. Notably, genes encoding *CXCL9, CXCL10* and *CXCL11* that mediate their effects by binding to the CXCR3 receptor were upregulated (>500 folds) upon infection with both RVFV strains. Several other chemokines, such as *CXCL1*, *CXCL5*, *CCL20*, etc., that aid leukocyte migration were downregulated in monocytes by Clone13 and the WT strains. Similarly, expression of genes encoding proinflammatory cytokines like interleukins *IL1A*, *IL1B* and *IL6* was downregulated in monocytes infected with both RVFV strains. Notable variations in fold changes were also observed between WT and Clone 13 infected monocytes. Expression of the gene encoding *CCL2*, a chemokine important for the recruitment of immune cells was upregulated in response to Clone 13 infection only. Similarly, expression of the *CSF1* gene encoding macrophage colony-stimulating factor was highly upregulated in Clone 13-infected monocytes. In contrast, expression of the *CSF3* gene encoding granulocyte colony-stimulating factor was strongly downregulated in WT-infected monocytes. Differences were also observed in the expression of genes encoding type-1-interferons, which exert potent antiviral activity. For instance, *IFNA1* expression was upregulated in WT and Clone 13-infected monocytes, whereas *IFNB1* expression was highly upregulated (>140 fold) in Clone 13-infected monocytes only (Figure 7(a,b)). Expression of STAT1 and STAT2 transcription factors was upregulated in monocytes by Clone 13 and WT strains. Collectively, these results indicate the ability of monocytes to sense either strains and respond by activating genes and pathways that drive innate immune response. However, fold changes of these genes suggest that the response in Clone 13-infected monocytes was relatively stronger compared to the response to the WT RVFV strain.

Clone 13 infection upregulates the expression of costimulatory molecules and chemokines in monocytes

Monocytes are important antigen-presenting cells that can activate virus-specific T cells. To assess the T cell-activating potential of monocytes induced by WT or Clone 13, the expressions of *CD80*, *CD40*, and *CD83* genes were assessed from the RNA-seq data. Differential gene expression data revealed that, compared to mock controls, *CD80* expression was higher in Clone 13-infected monocytes (~90-fold) than in WT-infected cells (10-fold). The expression of *CD40* and *CD83* was significantly upregulated after infection with Clone 13

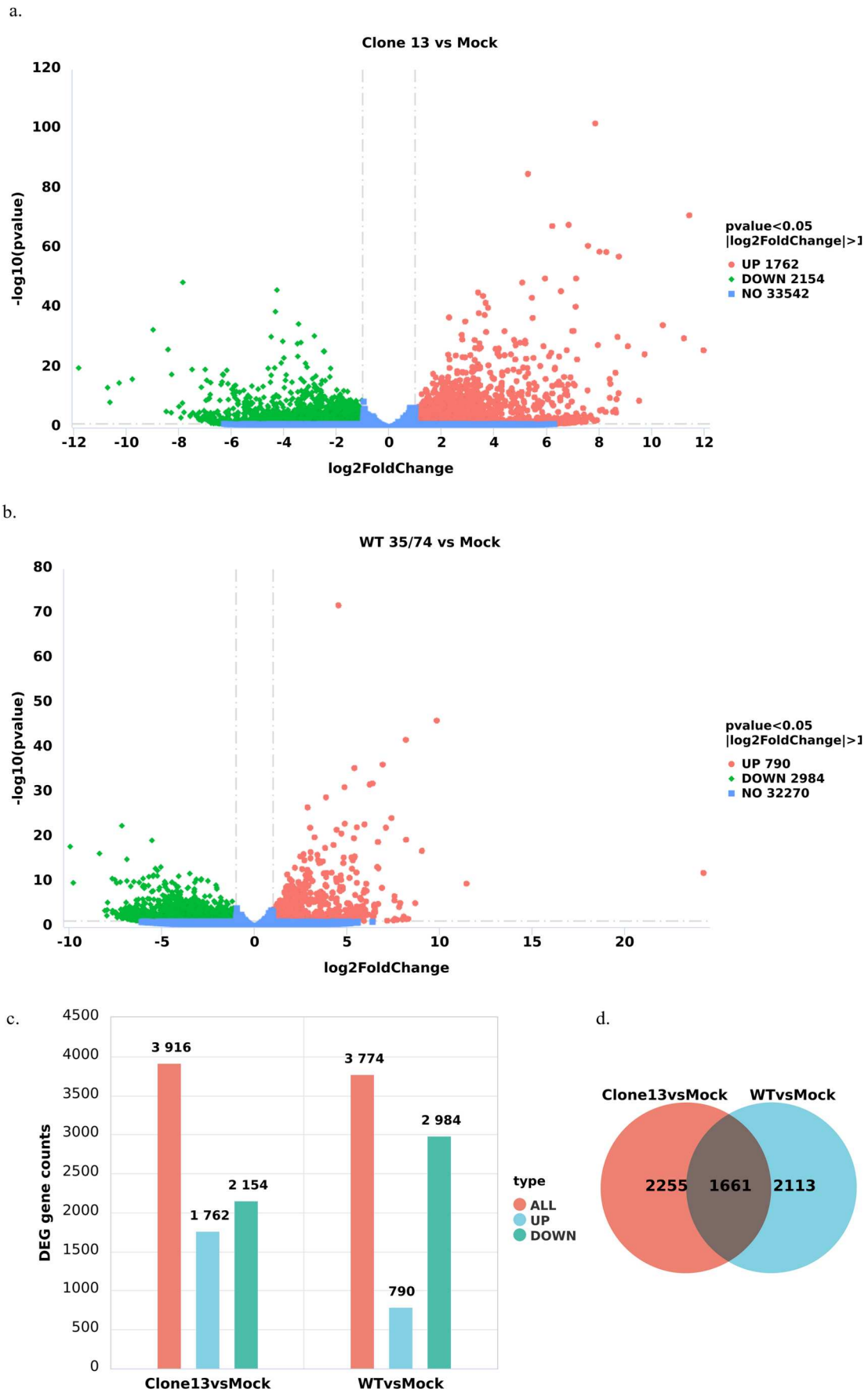

Figure 4. Differential gene expression in RVFV-inoculated monocytes. Volcano plots depict the enrichment of DEG (log_2fold change >1, *p*-Value < 0.05) in a. Clone 13 and b. WT-infected monocytes in comparison to mock-infection. c. The bar graph shows total DEG (red) and those that are up- (blue bar) and down- (green bar) regulated between these conditions. d. The Venn diagram shows DEG that are common for both infections (dark grey), Clone 13-specific (red) and WT (blue) -specific DEG.

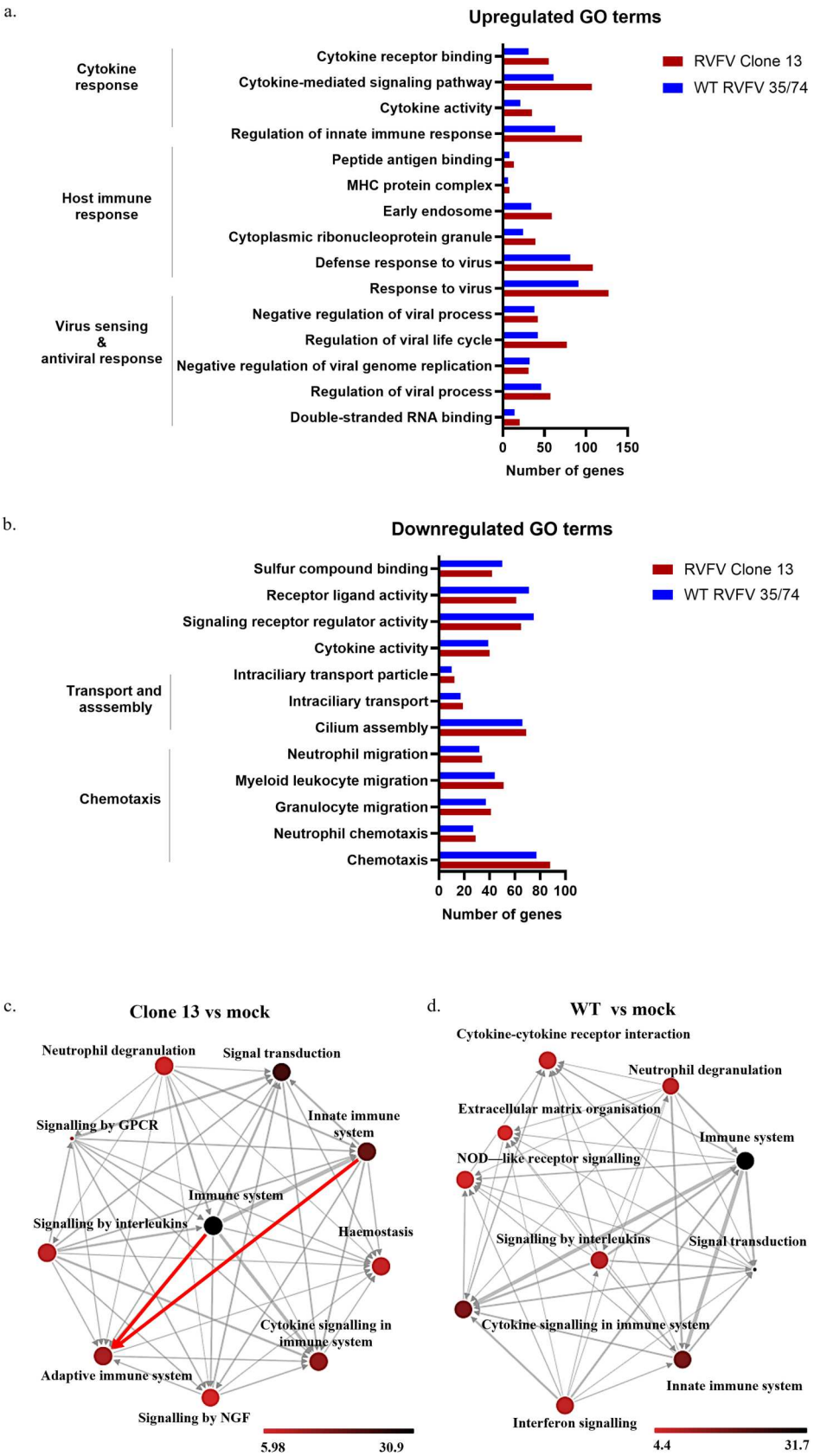

Figure 5. Total DEG filtered with parameters $|\log_2$ fold change$| > 1$ and $p < 0.05$ of Clone 13 or WT-infected monocytes relative to mock, expressed as a bar graph and interaction network. a. Upregulated GO terms and b. Downregulated GO terms in Clone 13 and RVFV 35/74 infected cells were compared to mock-infection. The total number of DEG associated with the given GO term for Clone 13 (red) and WT virus (blue) infection is shown on the *X*-axis. Network analysis of the highest annotated DEG for c. Clone 13 and d. WT infection. The link between the innate immune system and the adaptive immune system is highlighted in red. Each node represents a functional category, and colour represents the percentage of significant DEG annotated in this category. The size of the node indicates the *p*-value of the category; a larger node indicates high statistical significance. Edges show the functional categories with genes in common. Edge width is proportional to the number of genes in common. Legend represents the gradient of DEG annotation percentage.

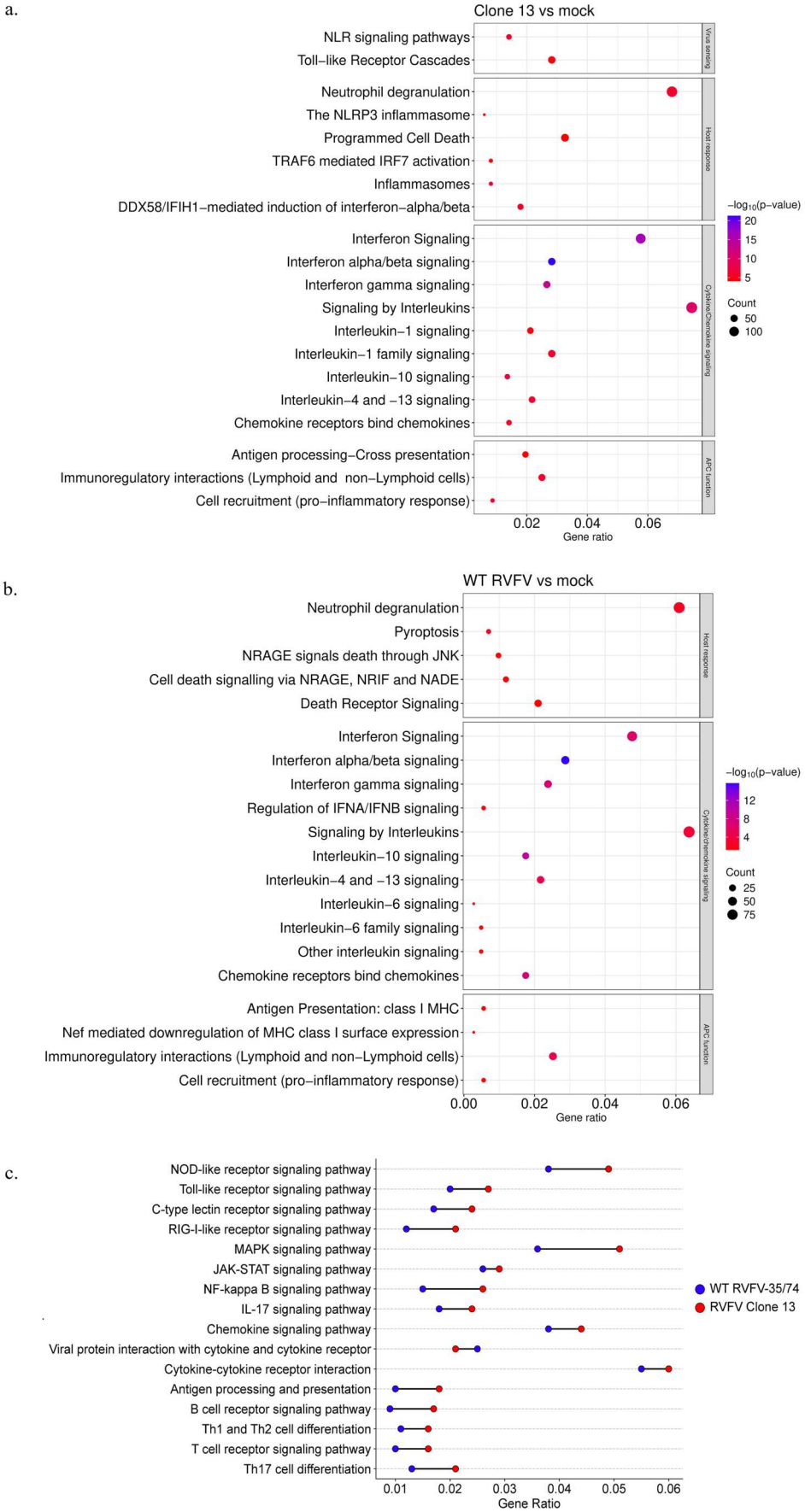

Figure 6. Reactome pathways enriched using common DEG a. Clone 13 and b. RVFV 35/74 infection was expressed as a scatter plot. The dot size indicates gene count and the colour indicates *p*-value. The *p*-values range from red colour indicating the least significant *p*-value, and violet colour for the highest significant *p*-value c. Gene ratios for KEGG immune pathways were compared for Clone 13-(red dots) and WT- (blue dots) infection and represented as a dumbbell plot. For a., b, c., the *x*-axis shows gene ratio to indicate pathways.

a.

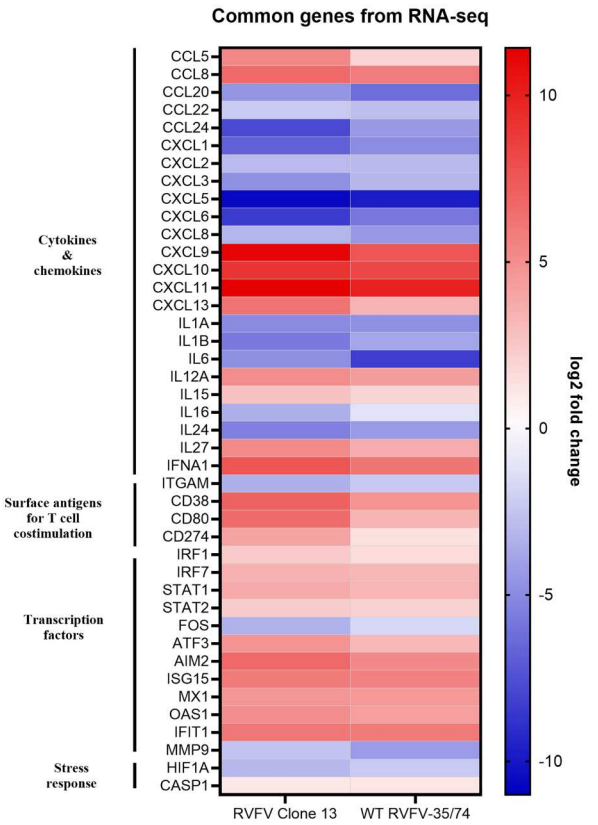

Surface marker	Log_2 fold change	
	RVFV Clone 13	WT RVFV-35/74
CD38	7.02	4.77
CD40	1.42	-
CD80	6.52	3.36
CD83	2.52	-

b.

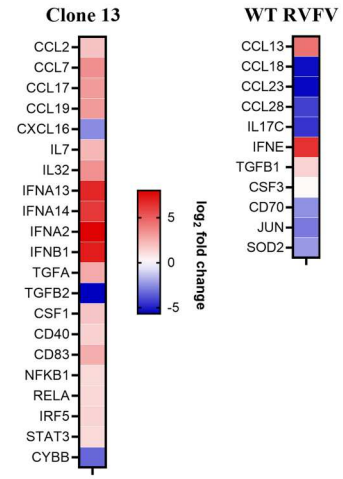

c.

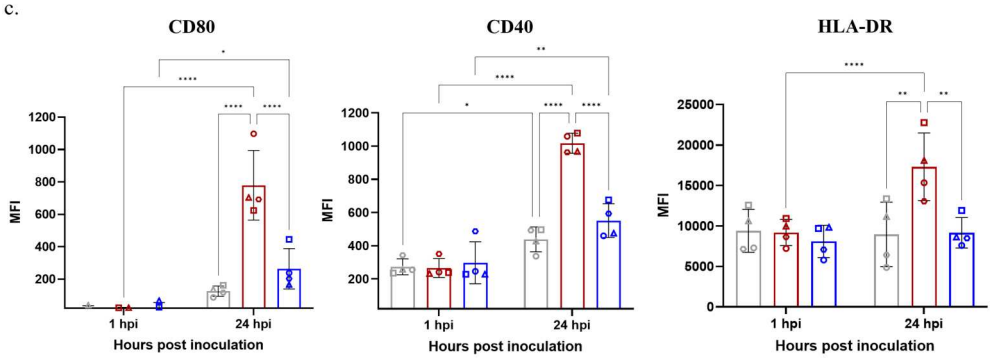

d.

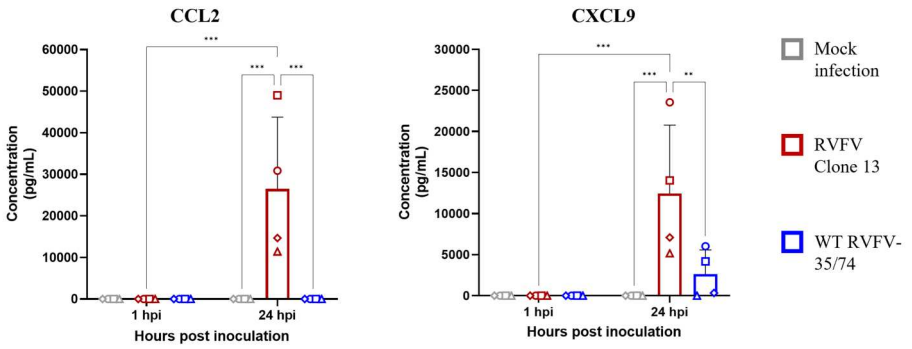

Figure 7. Heatmap showing log_2 fold change and $p < 0.05$ up- (red) or down-regulation (blue) for selected genes that are a. commonly expressed in WT and Clone 13 infections and b. genes specifically regulated with either WT or Clone 13 infection. Intensity of colour indicates the strength of regulation. Mean fluorescence intensities (MFI) of surface expression c. CD80, CD40 and HLA-DR on mock- (grey) Clone 13 (red) and WT (blue) infected monocytes were plotted from four blood donors (n = 4). d. Concentration (pg/mL) of chemokines CCL2 and CXCL9 in culture supernatants of mock- (grey), Clone 13- (red) or WT (blue) virus-infected monocytes at 1 and 24 hpi. Each symbol represents the average of two technical replicates from a blood donor ($n = 4$). Statistical significance was determined using two-way ANOVA and Tukey's multiple comparisons test. $*p < 0.05$; $**p < 0.01$; $***p < 0.001$; $****p < 0.0001$.

only (Figure 7(a,b)). Furthermore, flow cytometric analysis validated these findings, showing that surface expression (mean fluorescence intensity) of CD80, CD40 and HLA-DR was significantly higher on Clone 13-infected monocytes than in WT-infected cells compared to mock controls (Figure 7(c) & Supplementary figure S4). Similarly, the concentration of chemokines CCL2 and CXCL9 measured in the culture supernatants of Clone 13 and WT-infected monocytes showed that higher amounts of CCL2 were secreted by monocytes only in response to Clone 13 infection (Figure 7(d)). CXCL9 was detected in both supernatants; however, the concentration in Clone 13-infected monocyte cultures (12.5 ng/mL) was higher compared to that detected in supernatants of WT-infected monocytes (2.6 ng/mL; Figure 7(d)). The protein expression data for the selected genes were consistent with RNA-seq data. Collectively, these findings show that Clone 13 infection enhances chemokine secretion and T cell activation potential of monocytes more than WT RVFV infection.

Clone 13 and WT RVFV regulate unique functional pathways

A significant number of DEG were unique to either Clone 13-(2255) or WT-infected (2113) monocytes. Further GO and Reactome pathway analysis was done using these gene sets to identify unique biological processes and pathways that are affected by Clone 13 and WT infection. The enriched pathways were categorized into those involved in viral sensing, innate immune response, structural organization and cell survival (Figure 8). Notably, most pathways enriched by Clone 13-specific DEG were associated with viral sensing and host response to infection (Figure 8(a), Supplementary figure S5 & table S5). Enrichment of pathways like NLR-, CLR- and TLR-signalling cascades by Clone 13 specific gene set indicates transcriptional programmes regulating pathogen sensing, largely absent among top hits for WT-specific gene set (Figure 8). Similarly, pathways associated with interleukin signalling and inflammasome pathways driving host response to infection were primarily enriched with the Clone 13-specific gene set. In contrast, WT-specific DEG enriched top pathways were associated with structural organizations, cell survival and those regulating cell motility (Figure 8(b), Supplementary figure S5 & table S6). These results confirm that distinct transcriptional programmes associated with viral sensing and response to infection were more pronounced in Clone 13-infected monocytes, whereas the WT virus regulated programmes that affect cell survival.

Discussion

In the present study, we have confirmed that RVFV can infect mainly classical monocytes ($CD14^+$ $CD16^-$) within a human PBMC population. Previously, it was shown that RVFV can infect $THP\text{-}1^{PMA}$ differentiated macrophages, Raw 264.1 cells and human monocyte-derived macrophages *in vitro* [14,19,20]. Monocytes comprise approximately 10% of human PBMC, and function as immediate responders to infection and disease [21]. Inflammation results in the migration of classical monocytes from blood to specific organs where they differentiate into tissue-resident macrophages [22]. Infection of monocytes at the site of infection would be one way for the virus to travel systemically, eventually reaching target organs for massive virus replication. For example, Dengue virus and Zika virus can use monocytes to reach peripheral organs for further virus amplification [23–25].

Presumably, after initial replication at the sites of infection, RVFV enters the bloodstream to reach the main target organ, the liver. Hence, the early response to infection by circulating immune cells might be a critical factor in the pathogenesis of RVFV. Few studies have identified LRP1 as a potential cellular receptor along with a few attachment receptors for RVFV entry [26]. In addition, it was shown that LRP1 expression in hepatocytes was required for the development of severe hepatic disease in a mouse model [27]. After showing that monocytes among PBMC were the main targets of RVFV, it was intriguing to find that monocytes were also the major cell types expressing LRP1. Our findings suggest that the high cell surface expression of LRP1 on monocytes may be the reason for the observed cell tropism of RVFV in human PBMC. Nonetheless, the possibility that other viral receptors may also be involved in this process cannot be ruled out.

The ability of RVFV NSs to negatively impact innate immune responses by suppressing the gene expression of IFNβ is well established [28]. Hence, a comparison of monocyte responses to infection with WT versus NSs-deficient RVFV strains was our strategy to identify early events critical for pathogenesis. Early host responses were studied with 24 hpi as an appropriate time point, thus ensuring measurable and significant host response, while allowing virus replication to proceed. WT 35/74 and Clone 13 share a high amino acid sequence homology (>99%) for most viral proteins except for the NSs protein (31% homology). The absence of functional NSs did not affect the ability of Clone 13 to infect monocytes, as infection rates were comparable to those of WT RVFV. Although most of the transcriptional differences observed in this study could be attributed to the NSs, the possibility that some of these differences arise from the subtle amino acid variations in other viral proteins, such as the glycoproteins, cannot be excluded. A comparative analysis using isogenic virus strains would

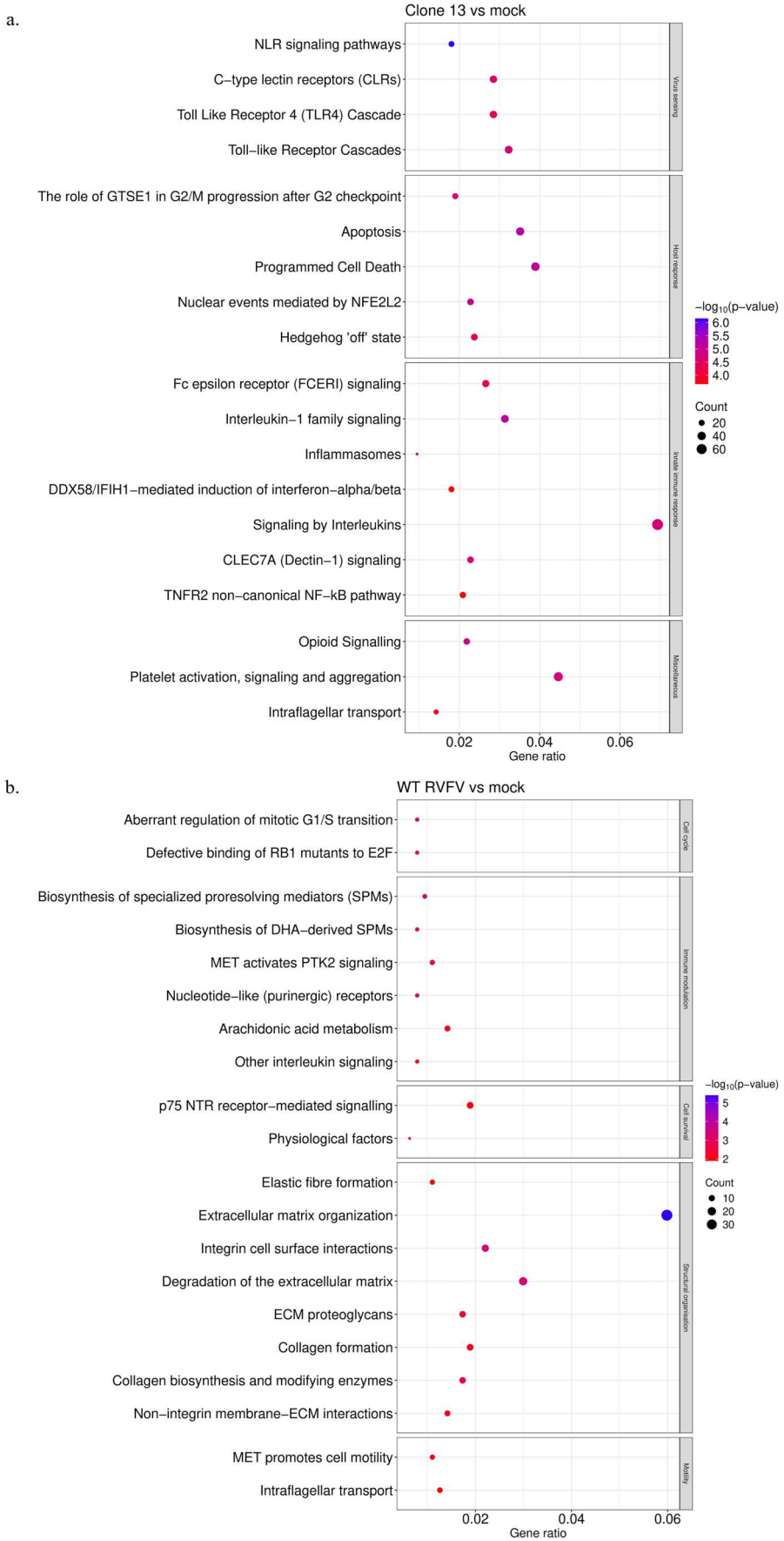

Figure 8. Reactome pathways enriched based on specific DEG from a. Clone 13- and b. WT-infected monocyte relative to mock-infection and is presented as a scatter plot. The *x*-axis represents gene ratio associated with pathways; dot size indicates gene count and colour indicates *p*-value. The *p*-values range from red colour, having the least significant *p*-value and violet colour for the highest significant *p*-value.

be the approach to resolve these effects. Assessment of infectivity by flow cytometry revealed that only a small monocyte fraction was infected. As the infected cells could not be sorted for RNA-seq analysis, the observed transcriptional changes could still be a combination of direct viral effects on infected monocytes and bystander response from uninfected cells. However, transcriptional changes induced by Clone 13 in monocytes were considerably different from that of WT RVFV-infected monocytes, both in terms of the overall number of DEG and the enriched GO terms and pathways associated with these DEG. Clone 13 infection upregulated the expression of more genes involved in the interferon response and pathways associated with control of viral infection in comparison to WT infection. Pathways regulating viral RNA sensing, like RIG-I-like receptor signalling (RLR) and NLR signalling pathways, which in turn regulate NF-κB signalling and expression of factors driving the innate immune response, were among the prominent hits associated with Clone 13 infection. Furthermore, Clone 13 induced robust expression of the *IFNB* gene, which was not the case in WT-infected monocytes. This is in agreement with the previous report of negative effects of NSs on *IFNB* expression [11]. Infection with Clone 13 and WT RVFV resulted in the expression of other chemokine and cytokine genes, including those encoding *CXCL9, CXCL10, CXCL11*, which are important for immune cell recruitment, activation and differentiation [29]. Upregulation of transcription factors such as STAT 1 and STAT 2 by either virus strains support the fact that virus sensing induces the activation of pathways that guide proinflammatory response. Furthermore, it is known that STAT1 regulates the differentiation of monocytes into M1-like macrophages, which form an important component of immune defence in tissues [30]. In contrast to infection with WT, Clone 13 infection induced the expression of cell surface markers involved in T cell activation by monocytes, like CD80, CD40 and HLA-DR, which was also reflected by a higher gene ratio for T- and B-cell activation signalling. These findings may explain the virulence associated with the WT virus, where the functional NSs resulted in diminished innate immune activation. Alternatively, Clone 13, lacking functional NSs, promotes viral sensing and antiviral defence mechanisms in monocytes, while the WT strain influences structural organization and cell mobility. The combinatorial effect of enhanced mobility and reduced antiviral defence mechanisms contributes to the pathogenesis of the WT strain [31]. Nevertheless, we also observed that genes encoding key proinflammatory factors such as IL-1β, IL-6 and several chemokines involved with chemotaxis and leukocyte migration are downregulated in monocytes by both Clone 13 and WT strains. The reason for this is unclear. It is likely that these factors are regulated independently of NSs and are influenced by other viral proteins. It has been demonstrated that nucleoprotein encoded by the S segment of severe fever with thrombocytopenia syndrome virus (SFTSV) exhibited suppressive effect on NF-KB signalling [32].

Monocytes with their antigen-presenting capabilities, could act as a bridge between innate and adaptive immune responses. Therefore, the gene expression data combined with flow cytometric data validating the expression of costimulatory molecules support our hypothesis that contact with monocytes during the early infection and the ensuing response may be one of the factors determining immunity to infection or dissemination and trafficking of the virus to primary target organs such as the liver. Collectively, we have demonstrated that both attenuated and WT strains of RVFV can infect human monocytes efficiently, which coincides with the expression of the virus receptor LRP1. However, the cellular response of monocytes to infection with either virus varies widely in relation to a functional NSs gene, which is absent in the Clone 13 strain. Absence of potent innate and subsequent adaptive immune responses seen after infection with the WT strains may contribute to virus dissemination, leading to full-blown infections and high viral loads. Further studies are required to validate the impact of transcriptional changes identified in our RNA-seq analysis on the function of monocytes. Although we could demonstrate that gene expression data is consistent with protein expression for selected genes, it must be noted that RVFV NSs is known to block mRNA export from the nucleus and hence the gene expression changes may not always be reflected at the protein level [33,34]. Therefore, this limitation must be considered while validating these findings.

Acknowledgements

The authors would like to thank Dr. Marie Flamand and Dr. Michèle Bouloy from the Institut Pasteur for providing RVFV Clone 13 used in this study.

Author contributions

C.K.P., G.F.R., P.J.W.S., A.D.M.E.O. supervised the project. G.F.R. and A.D.M.E.O. acquired the grants. C.K.P., G.F.R. conceptualized the project. C.K.P, G.F.R., N.N., P.J.W.S. designed the experiments. N.N., J.F. performed the experiments, C.K.P, N.N. performed data analysis. N.N., C.K.P., G.F.R. prepared the manuscript. All authors edited and reviewed the manuscript before publication.

Disclosure statement

No potential conflict of interest was reported by the authors.

Funding

This research was funded by the Deutsche Forschungsgemeinschaft (DFG, German Research Foundation)—398066876/GRK 2485/2. This publication was supported by the Open Access Publication Fund of the University of Veterinary Medicine Hannover, Foundation.

Data availability statement

The data relevant for this publication were presented as figures in this research article. Any additional data required will be made available upon request.

References

[1] Daubney RH, Hudson JR, Garnham PC. Enzootic hepatitis or Rift Valley fever. An undescribed virus disease of sheep cattle and man from East Africa. J Pathol Bacteriol. 1931;34:545–579. doi:10.1002/path.1700340418

[2] Schwentker FF, Rivers TM. Rift Valley fever in man: report of a fatal laboratory infection complicated by thrombophlebitis. J Exp Med. 1934;59(3):305–313. doi:10.1084/jem.59.3.305

[3] Nair N, Osterhaus ADME, Rimmelzwaan GF, et al. Rift Valley fever virus – infection, pathogenesis and host immune responses. Pathogens. 2023;12(9):1174. doi:10.3390/pathogens12091174

[4] Odendaal L, Davis AS, Venter EH. Insights into the pathogenesis of viral haemorrhagic fever based on virus tropism and tissue lesions of natural Rift Valley fever. Viruses. 2021;13(4):709. doi:10.3390/v13040709

[5] Connors KA, Hartman AL. Advances in understanding neuropathogenesis of Rift Valley fever virus. Annu Rev Virol. 2022;9(1):437–450. doi:10.1146/annurev-virology-091919-065806

[6] Nsengimana I, Juma J, Roesel K, et al. Genomic epidemiology of Rift Valley fever virus involved in the 2018 and 2022 outbreaks in livestock in Rwanda. Viruses. 2024 Jul 17;16(7):1148. doi:10.3390/v16071148

[7] Gaudreault NN, Indran SV, Balaraman V, et al. Molecular aspects of Rift Valley fever virus and the emergence of reassortants. Virus Genes. 2019 Feb;55(1):1–11. doi:10.1007/s11262-018-1611-y

[8] Leger P, Nachman E, Richter K, et al. NSs amyloid formation is associated with the virulence of Rift Valley fever virus in mice. Nat Commun. 2020 Jul 1;11(1):3281. doi:10.1038/s41467-020-17101-y

[9] Li S, Zhu X, Guan Z, et al. NSs filament formation is important but not sufficient for RVFV virulence in vivo. Viruses. 2019;11(9):834. doi:10.3390/v11090834

[10] Bouloy M, Janzen C, Vialat P, et al. Genetic evidence for an interferon-antagonistic function of Rift Valley fever virus nonstructural protein NSs. J Virol. 2001 Feb;75(3):1371–1377. doi:10.1128/JVI.75.3.1371-1377.2001

[11] Billecocq A, Spiegel M, Vialat P, et al. NSs protein of Rift Valley fever virus blocks interferon production by inhibiting host gene transcription. J Virol. 2004 Sep;78(18):9798–9806. doi:10.1128/JVI.78.18.9798-9806.2004

[12] Muller RS, Saluzzo JF, Lopez N, et al. Characterization of clone 13, a naturally attenuated avirulent isolate of Rift Valley fever virus, which is altered in the small segment. Am J Trop Med Hyg. 1995;53(4):405–411. doi:10.4269/ajtmh.1995.53.405

[13] Gommet C, Billecocq A, Jouvion G, et al. Tissue tropism and target cells of NSs-deleted Rift Valley fever virus in live immunodeficient mice. PLoS Negl Trop Dis. 2011 Dec;5(12):e1421. doi:10.1371/journal.pntd.0001421

[14] McElroy AK, Nichol ST. Rift valley fever virus inhibits a pro-inflammatory response in experimentally infected human monocyte derived macrophages and a pro-inflammatory cytokine response may be associated with patient survival during natural infection. Virology. 2012 Jan 5;422(1):6–12. doi:10.1016/j.virol.2011.09.023

[15] Prajeeth CK, Zdora I, Saletti G, et al. Immune correlates of protection of the four-segmented Rift Valley fever virus candidate vaccine in mice. Emerging Microbes Infect. 2024;13(1):2373313. doi:10.1080/22221751.2024.2373313

[16] Drosten C, Gottig S, Schilling S, et al. Rapid detection and quantification of RNA of Ebola and Marburg viruses, Lassa virus, Crimean-Congo hemorrhagic fever virus, Rift Valley fever virus, dengue virus, and yellow fever virus by real-time reverse transcription-PCR. J Clin Microbiol. 2002;40(7):2323–2330. doi:10.1128/JCM.40.7.2323-2330.2002

[17] Tang D, Chen M, Huang X, et al. SRplot: a free online platform for data visualization and graphing. PLoS One. 2023;18(11):e0294236. doi:10.1371/journal.pone.0294236

[18] Prieto C, Barrios D. RaNA-Seq: interactive RNA-Seq analysis from FASTQ files to functional analysis. Bioinformatics. 2019;36(6):1955–1956.

[19] Zhu X, Guan Z, Fang Y, et al. Rift Valley fever virus nucleoprotein triggers autophagy to dampen antiviral innate immune responses. J Virol. 2023 Apr 27;97(4):e0181422. doi:10.1128/jvi.01814-22

[20] Makola RT, Kgaladi J, More GK, et al. Lithium inhibits NF-κB nuclear translocation and modulate inflammation profiles in Rift Valley fever virus-infected Raw 264.7 macrophages. Virol J. 2021 Jun 4;18(1):116. doi:10.1186/s12985-021-01579-z

[21] Mildner A, Kim KW, Yona S. Unravelling monocyte functions: from the guardians of health to the regulators of disease. Discov Immunol. 2024;3(1):kyae014. doi:10.1093/discim/kyae014

[22] Jakubzick CV, Randolph GJ, Henson PM. Monocyte differentiation and antigen-presenting functions. Nat Rev Immunol. 2017 Jun;17(6):349–362. doi:10.1038/nri.2017.28

[23] Hwang EH, Hur GH, Koo BS, et al. Monocytes as suitable carriers for dissemination of dengue viral infection. Heliyon. 2022 Oct;8(10):e11212. doi:10.1016/j.heliyon.2022.e11212

[24] Hernandez-Sarmiento LJ, Valdes-Lopez JF, Urcuqui-Inchima S. Zika virus infection suppresses CYP24A1 and CAMP expression in human monocytes. Arch Virol. 2024 Jun 6;169(7):135. doi:10.1007/s00705-024-06050-2

[25] Michlmayr D, Andrade P, Gonzalez K, et al. CD14(+)CD16(+) monocytes are the main target of Zika virus infection in peripheral blood mononuclear cells in a paediatric study in Nicaragua. Nat

Microbiol. 2017 Nov;2(11):1462–1470. doi:10.1038/s41564-017-0035-0

[26] Ganaie SS, Leung DW, Hartman AL, et al. Advances in virus research. Adv Virus Res. 2023;117:121–136. doi:10.1016/bs.aivir.2023.09.001

[27] Schwarz MM, Ganaie SS, Feng A, et al. Lrp1 is essential for lethal Rift Valley fever hepatic disease in mice. Sci Adv. 2023 Jul 14;9(28):eadh2264. doi:10.1126/sciadv.adh2264

[28] Wang X, Yuan Y, Liu Y, et al. Arm race between Rift Valley fever virus and host. Front Immunol. 2022;13:1084230. doi:10.3389/fimmu.2022.1084230

[29] Tokunaga R, Zhang W, Naseem M, et al. CXCL9, CXCL10, CXCL11/CXCR3 axis for immune activation – A target for novel cancer therapy. Cancer Treat Rev. 2018 Feb;63:40–47. doi:10.1016/j.ctrv.2017.11.007

[30] Collins-McMillen D, Stevenson EV, Kim JH, et al. Human cytomegalovirus utilizes a nontraditional signal transducer and activator of transcription 1 activation cascade via signaling through epidermal growth factor receptor and integrins to efficiently promote the motility, differentiation, and polarization of infected monocytes. J Virol. 2017 Dec 15;91(24):e00622-17. doi:10.1128/JVI.00622-17

[31] Bamia A, Marcato V, Boissiere M, et al. The NSs protein encoded by the virulent strain of Rift Valley fever virus targets the expression of Abl2 and the actin cytoskeleton of the host, affecting cell mobility, cell shape, and cell-cell adhesion. J Virol. 2020 Dec 9;95(1):e01768-20. doi:10.1128/JVI.01768-20

[32] Qu B, Qi X, Wu X, et al. Suppression of the interferon and NF-κB responses by severe fever with thrombocytopenia syndrome virus. J Virol. 2012 Aug;86(16):8388–8401. doi:10.1128/JVI.00612-12

[33] Copeland AM, Van Deusen NM, Schmaljohn CS. Rift valley fever virus NSS gene expression correlates with a defect in nuclear mRNA export. Virology. 2015 Dec;486:88–93. doi:10.1016/j.virol.2015.09.003

[34] Pinkham C, Dahal B, de la Fuente CL, et al. Alterations in the host transcriptome in vitro following Rift Valley fever virus infection. Sci Rep. 2017 Oct 30;7(1):14385. doi:10.1038/s41598-017-14800-3